

# Screening Phenomena on Oxide Surfaces and Its Implications for Local Electrostatic and Transport Measurements

Sergei V. Kalinin\*<sup>†</sup> and Dawn A. Bonnell<sup>‡</sup>

*Condensed Matter Sciences Division, Oak Ridge National Laboratory, Oak Ridge, Tennessee 37831, and Department of Materials Science and Engineering, The University of Pennsylvania, Philadelphia, Pennsylvania 19104*

*Received November 26, 2003; Revised Manuscript Received January 7, 2004*

## ABSTRACT

The determination of local electrical, electrostatic, and transport properties of materials by ambient scanning probe microscopy (SPM) is shown to be strongly affected by the adsorption of charged species. Associated surface screening results in new phenomena including potential retention above the Curie temperature on ferroelectric surfaces and potential inversion on grain boundary–surface junctions. Implications of screening for a variety of SPMs including piezoresponse force microscopy and transport measurements in carbon nanotubes and molecular electronic devices are discussed.

In recent years, scanning probe microscopy techniques such as electrostatic force microscopy (EFM) and scanning surface potential microscopy (SSPM), (also known as Kelvin probe force microscopy (KPFM)) have been extensively used for the imaging and quantification of local electrical properties of materials, including the doping level, grain boundaries, dislocations, and defects in semiconductors,<sup>1,2</sup> ferroelectric domains,<sup>3,4</sup> and photoinduced,<sup>5,6</sup> thermal,<sup>7,8</sup> and transport phenomena.<sup>9</sup> A significant effort has addressed the imaging mechanisms of these techniques including tip shape, feedback and cantilever effects, and resolution limits, paving the way for the quantitative interpretation of SPM data in terms of local materials properties. In most cases, measured surface potentials were interpreted directly in terms of the bulk properties, and little or no attention was paid to the state of the surface (e.g., the presence of mobile adsorbates that is inevitable under ambient conditions). The presence of a surface water layer is well known in SPM;<sup>10</sup> it affects such diverse phenomena as capillary tip–surface forces and tip-induced local electrochemical processes such as nanooxidation.<sup>11,12</sup> Despite the fact that the effect of mobile charges on EFM imaging was demonstrated as early as 1993,<sup>13</sup> little is known of the mechanisms of surface screening and its implications on electrostatic measurements by SPM because the observation of screening behavior requires dynamic measurements under an applied field or a variable temperature or atmosphere.<sup>14</sup>

Here we demonstrate that surface adsorption can drastically change local electrostatic properties on oxide surfaces and give rise to new physical phenomena, including potential inversion at grain boundary–surface junctions and on ferroelectric surfaces. Surface screening not only changes the magnitude of observed potential features but also can change the sign, leading to the potentially erroneous interpretation of SPM data in terms of materials parameters. Implications of universal screening are illustrated for three classes of problems, including conductive oxide surfaces, grain boundary–surface junctions in polycrystalline oxides, and ferroelectric surfaces.

**Conductive Surfaces.** Evidence for the presence of mobile charges on oxide surfaces can be inferred from charge deposition experiments. It has long been recognized that a metallic tip can be used to deposit charge on an insulating surface in a processes called contact electrification. The evolution of charge due to diffusion can be observed by EFM or SSPM, providing data on the mobility and diffusion coefficient of surface charges.<sup>15–17</sup> Figure 1a illustrates the potential of charge deposited on a degenerately *n*-doped SrTiO<sub>3</sub> surface by a biased metallic AFM tip. Strikingly, the surface retains local charge even though the material per se is metallic (resistivity 0.01 Ω cm). The deposited charges are mobile, resulting in the lateral spreading of the potential profile on the time scale of tens of minutes. This surface charging can be attributed to the difference in conductivity between the surface and the bulk or to the presence of mobile adsorbates. However, the conductive nature of the surface

\* Corresponding author. E-mail: sergei2@ornl.gov.

<sup>†</sup> Oak Ridge National Laboratory.

<sup>‡</sup> The University of Pennsylvania.

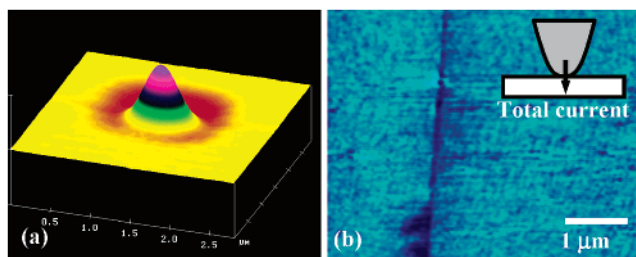


**Figure 1.** (a) SSPM image of a conductive SrTiO<sub>3</sub> surface 10 min after contact electrification by an AFM tip at +5-V and -5-V biases with a 20-min interval (image is inverted). During the first electrification step, the surface was positively charged. Deposited positive charge diffused laterally with time, and the second electrification step resulted in much sharper negative feature in the center, resulting in a ringlike structure. This contact electrification/charge diffusion illustrates the presence of low-mobility surface charges. (b) Conductive AFM image of the bicrystal surface with a grain boundary. Nonzero tip-surface current measured far from the grain boundary demonstrates that the surface is conductive.

can be confirmed by the conductive atomic force microscopy (AFM) image of the same region with the grain boundary as shown in Figure 1b. The grain boundary is associated with a higher resistivity region providing a reference point for AFM resistivity measurements, but the surface itself is clearly conductive. Therefore, charge retention and the subsequent dissipation of the mobile charge can be explained only by the presence of a low-mobility conductive layer on the nominally metallic surface.

**Grain Boundaries.** Evidence for the presence of mobile surface charges can be obtained from the observations of the dynamic potential behavior at charged defects such as grain boundaries. Well-defined grain boundaries in SrTiO<sub>3</sub> bicrystals<sup>18</sup> were studied using standard AFM and SSPM<sup>19</sup> as illustrated in Figure 2. The surface potential exhibits a

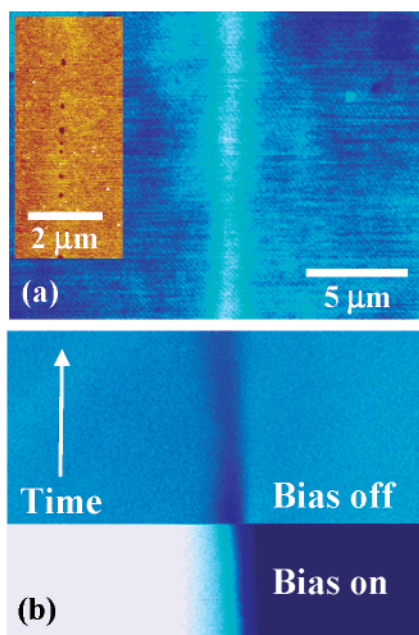


**Figure 2.** (a) Equilibrium surface potential at the SrTiO<sub>3</sub> bicrystal grain boundary. The inset shows surface topography. (b) Grain boundary potential evolution in the turn-off experiment. The arrow indicates the time direction. Charge and potential distributions at (c) pristine and (d) screened grain boundary surface junctions.

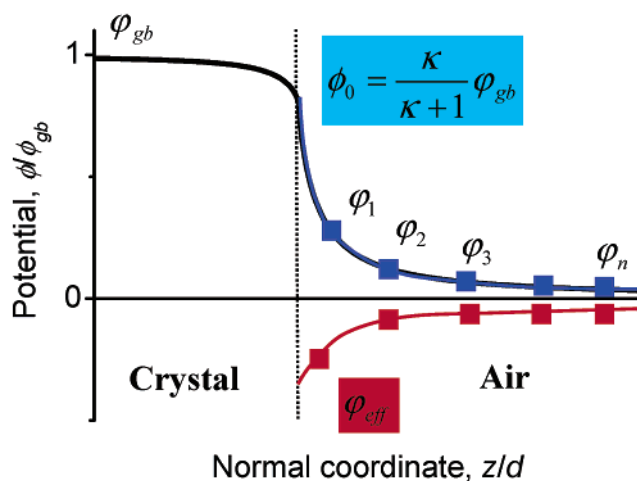
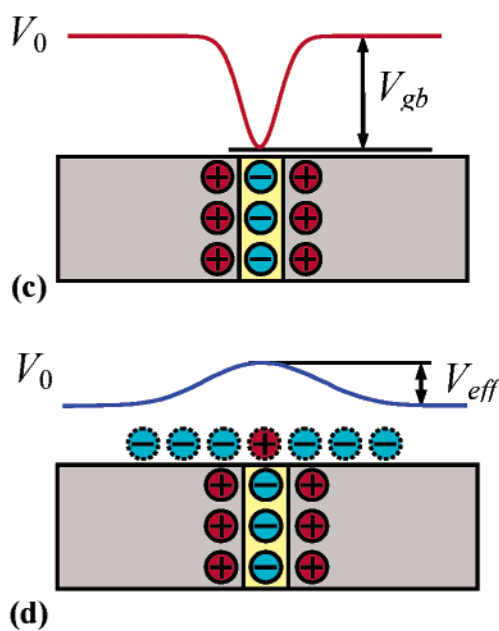


**Figure 3.** Potential distribution above the surface-interface junction for ideal (blue) and real (red) termination. Measured by SSPM are potential values at different tip-surface separations that can be extrapolated to the value at the tip-surface junction,  $\phi_0$ , using the analytical model.<sup>20</sup> For ideal termination, the tip-surface junction potential is directly related to the grain boundary potential in the bulk. For the realistic surface with mobile charges, there is no simple relationship between potential at the junction and potential in the bulk.

distinct feature of width  $\sim 700$  nm and magnitude  $\sim 20$  mV associated with the grain boundary. To determine the intrinsic materials properties from SPM data, a detailed analysis of the image-formation mechanism was developed.<sup>20</sup> The potential within the crystal is almost constant, decreasing only to  $\kappa/(\kappa + 1)$  of its bulk value at the surface-interface junction, and decreases rapidly in air (Figure 3). The quantification of both the EFM and SSPM results leads to a depletion width of  $d_{sc} \approx 200$  nm and a potential of  $\phi_{gb} \approx 30$  mV for the grain boundary (i.e., close to the values measured



directly). In comparison, corresponding values for this interface determined from transport and capacitance measurements are  $\sim 0.6$  V and  $\sim 15$  nm.<sup>21</sup> The discrepancy between SSPM results and conventional measurements was attributed to the surface damage and charge accumulation at the surface-interface junction and the finite resolution of the SSPM, resulting in the widening and lowering of the potential profile.

However, none of these considerations explains the positive sign of the grain boundary potential feature as observed by SSPM. In the *n*-doped material, this corresponds to an accumulation-type grain boundary, which can account for the small value of the grain boundary potential limited by the separation between the donor levels and the bottom of the conduction band. However, using SSPM imaging under applied bias, we find that the grain boundary is unambiguously associated with a potential barrier as illustrated in Figure 2b (bottom) and is therefore of the depletion type and must be negatively charged. To rationalize these observations, we introduce a screening model for the surface-interface junction as shown in Figure 2c and d. The accumulation of charged adsorbates at the surface-interface junction results in the widening of the grain boundary potential feature and, most notably, in the sign inversion. To verify this hypothesis, we attempted to remove the screening charges. In the first case, the application of lateral bias across the interface results in the high lateral field in the interface region ( $\sim 10^7$  V/m). The electrostatic forces induced by the field swipe the screening charges from the surface-interface junction area. After the bias is switched off, the true sign of the grain boundary is observed, as illustrated in Figure 2b (top). This potential distribution is metastable, and the accumulation of screening charges reduces the magnitude of the negative feature with subsequent sign reversal. Associated relaxation times are large (30 min to several hours) and strongly depend on the surface treatment prior to the experiment. It can be argued that this effect can be attributed to charge trapping at the interface; however, the retention time is much larger than can be expected for typical interface states, and no such relaxation process was observed in the impedance spectroscopy data.<sup>21</sup>

An additional approach to determining the screening dynamics utilizes temperature variation. In this case, increasing the temperature results in an increase of the apparent interface potential in polycrystalline  $\text{Ba}_x\text{Sr}_{1-x}\text{O}_3$  as illustrated in Figure 4. On decreasing the temperature, the sign of the grain boundary potential feature is inverted; the relaxation time to the equilibrium positive value is  $\sim 30$  min.

These results illustrate that ambient screening can affect measurements of the grain boundary potential barrier and depletion width. Even though the potential on the surface-interface junction can be determined reliably from the distance dependence of the grain boundary potential contrast, it is not simply related to the potential of the grain boundary in the bulk. In fact, even the sign of the potential can be determined erroneously. In the case when surface screening dominates, the depletion width measured by SSPM corresponds to the Debye length of the screening charges on the

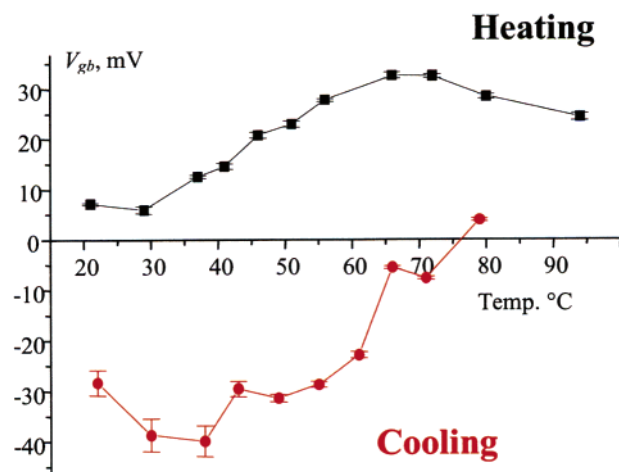


**Figure 4.** Temperature dependence of the grain boundary potential in polycrystalline barium–strontium titanate on heating (black) and cooling (red) (courtesy of F. Weibel).

surface, and observed potential values are determined by the thermodynamics of the screening process. Additional analysis is required to establish the relationship with intrinsic materials properties.

**Ferroelectric Materials.** In ferroelectric and piezoelectric materials, the discontinuity of the normal polarization component gives rise to a surface charge density,  $\sigma = \mathbf{P} \cdot \mathbf{n}$ , where  $\mathbf{P}$  is the polarization vector and  $\mathbf{n}$  is the unit normal. Polarization charge alters the electrical properties of the surface, which can be detected by electrostatic SPMs, providing an approach for local domain imaging. Similar to grain boundaries in oxides, the surface potential measured by SSPM is not only smaller but also has the opposite sign to that expected from the polarization orientation.<sup>22,23</sup>

Our first insight into this behavior was obtained from the potential measurements on static  $\text{BaTiO}_3$  surfaces. The measured potential was found to be uniform within the domain, with a potential difference between domains of opposite polarity of 150 mV. This potential difference corresponds to a dipole layer with 0.2-nm thickness, a dielectric constant of  $\kappa = 80$ , and a charge density of 0.25 C/m<sup>2</sup>, which is consistent with a screening water layer.<sup>22</sup> However, because of the large uncertainties associated with the quantitative interpretation of SPM data and the general lack of understanding of the fundamental mechanisms of polarization screening at ferroelectric surfaces, these considerations alone are insufficient to validate this picture. Similar to the case of grain boundaries, fundamental insight into charge behavior on ferroelectric surfaces can be obtained only from the observation of dynamic phenomena.

The temperature dependence of the polarization-related surface potential is illustrated in Figure 5. The surface of the ferroelectric phase is characterized by corrugations due to the lattice mismatch (Figure 5a); the surface potential image also exhibits potential variations due to the differences in surface charge density between  $c^+$  (upward),  $c^-$  (downward), and *a* (in-plane) domains (Figure 5b). Above the Curie temperature ( $T_c = 130$  °C), ferroelectric polarization disappears, as indicated by the absence of surface corrugations

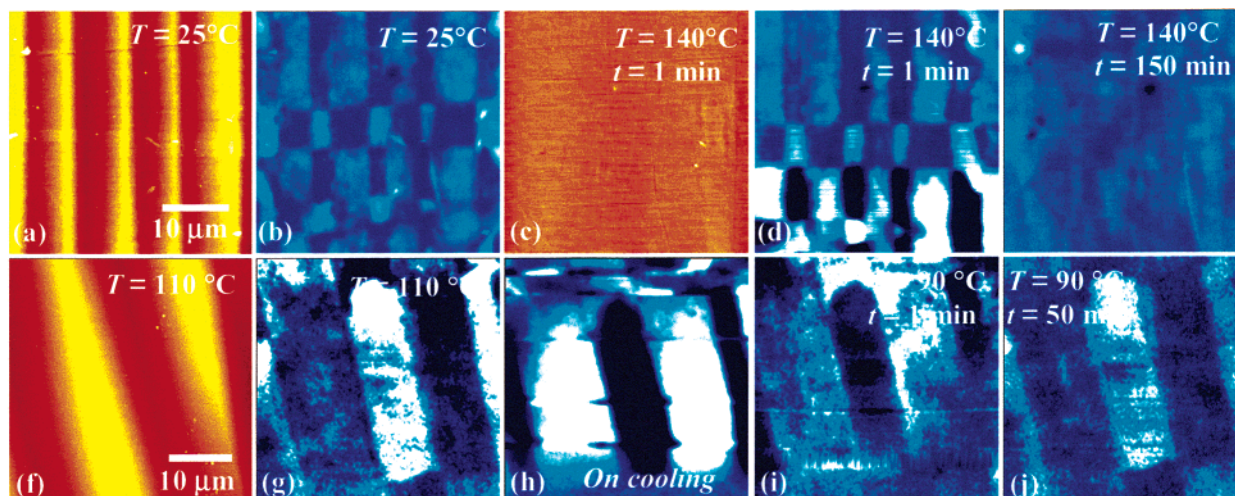


**Figure 5.** Surface topography (red) and potential distribution (blue) at the BaTiO<sub>3</sub>(100) surface (a, b) before the ferroelectric phase transition at 25 °C, (c, d) 1 min after transition, and (e) after 2.5 h of annealing at 140 °C. The scales are (b) 0.1 V, (d) 0.5 V, and (e) 0.1 V. (f) Surface topography and (g) surface potential of the ferroelectric domain structure on the BaTiO<sub>3</sub>(100) surface at  $T = 110$  °C. Surface potential (h) during cooling from 110 to 90 °C, (i) at 90 °C, and (j) after annealing at 90 °C for 50 min.

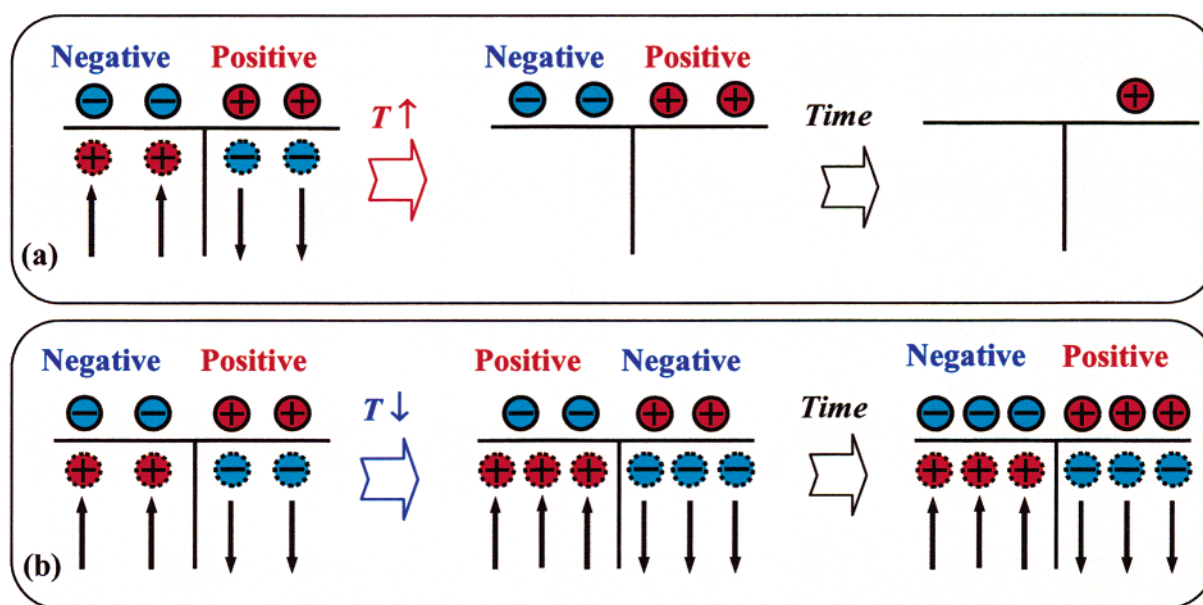


**Figure 6.** Charge dynamics on the ferroelectric surface on (a) heating and (b) cooling illustrating the interplay between fast polarization charge and slow screening charge dynamics as described in the text.

(Figure 5c). Unexpectedly, this is not the case for the potential. The morphology of the potential features remains essentially the same (cf. Figure 5, parts b and d); however, at the transition, the potential amplitudes grow by almost 2 orders of magnitude. As can be seen from Figure 5d (the image was acquired from bottom to top 4 min after the transition; total acquisition time, 11 min), the potential amplitude decays with time. The surface potential amplitude after annealing at 140 °C for 2.5 h is very small ( $\sim 2\text{--}5$  mV), and the potential distribution is almost random.

Reciprocal behavior is observed on decreasing the temperature (Figure 5f–j). After a temperature decrease from 110 to 90 °C, the topographic structure does not change significantly (Figure 5f), but the domain contrast inverts (Figure 5g and h) (i.e., a positive  $c$  domain becomes negative). The potential difference between the domains

decreases with time, passing through an isopotential point corresponding to zero domain potential contrast (Figure 5i) and finally establishing an equilibrium value (Figure 5j).

This behavior implies that the sign and magnitude of the measured surface potential are not determined only by the polarization charge. A more complex picture for surface potential behavior emerges, as illustrated in Figure 6a and b. The surface potential has the sign of the screening charges and is the reverse of that expected from the polarization orientation (i.e.,  $c^+$  domains are negative and  $c^-$  domains are positive on the SSPM image). Increasing the temperature results in a decrease in polarization bound charge, leaving some of the screening charge uncompensated, thus increasing the effective surface potential. In the limit of a ferroelectric phase transition, polarization charge disappears, leaving the screening charge completely uncompensated (Figure 6a).

This potential distribution is unstable and relaxes with time to a new equilibrium surface potential ( $T < T_c$ ) or a featureless potential distribution ( $T > T_c$ ).<sup>22</sup> On decreasing the temperature, spontaneous polarization increases, and for a short period of time, the domain's potential sign is determined by the polarization charge rather than the screening charge (temperature-induced domain potential inversion) (Figure 6b).<sup>23</sup> Under isothermal conditions, polarization and screening charges equilibrate, and the potential establishes an equilibrium value.

Noteworthy is that the characteristic time for surface potential relaxation on the ferroelectric surface ( $\sim 30$  min) is close to the relaxation time of the grain boundary potentials for the SrTiO<sub>3</sub> surface, suggesting a similarity between the mobile charge dynamics and screening phenomena on oxide surfaces.

**Implications.** These examples illustrate that surface potential measurements on oxide surfaces, as diverse as ferroelectrics, grain boundary, or charging phenomena, are strongly affected and in some cases are governed by the surface water layer and mobile charges. This layer significantly affects mechanical and electric properties of the tip–surface junction, providing higher effective conductivity and a larger effective contact area compared with those of the clean surface. This will affect the imaging mechanism and measured contrast in scanning probe techniques based on current or electro-mechanical detection (e.g., conductive AFM and scanning spreading resistance microscopy, piezoresponse force microscopy, etc.) The anomalous behavior of PFM contrast under vacuum conditions reported by Zheng et al.<sup>24</sup> can be rationalized by the elimination of the conductive surface layer and the formation of the dielectric gap between the tip and the surface. At the same time, the absence of conductive layer will significantly affect the fundamental physical phenomena on the ferroelectric surfaces (e.g., in vacuum, ferroelectric polarization can be expected to be screened by intrinsic charge carriers rather than mobile adsorbates, giving rise to completely different thermal behavior).

The mobile charge effects are even more pronounced for the noncontact electrostatic SPM techniques. In this case, the adsorption of the charge species from the ambient significantly affects the intrinsic potential distribution on the surface. Examples above illustrate that for several oxide systems the surface potential is inverse in sign to the corresponding bulk value because of specific adsorption. In other cases, the formation of a conductive water layer will reduce the measured potential amplitude and result in the broadening of features. The general approach to avoid this complication is the use of hydrophobic surfaces or measurements under controlled atmospheric conditions or in vacuum.

Finally, mobile charge effects are also important for the SPM-based transport measurements. In these techniques, a moving SPM tip acts as a voltage sensor probing the potential distribution created by a bias applied between macroscopic electrical contacts, thus allowing spatially resolved transport measurements. Clearly, a conductive water layer on the surface provides an alternative current path. The redistribution of the charges in the vicinity of resistive regions (e.g., in lateral transport across grain boundaries and electroactive interfaces) increases the observed profile width, limiting

resolution. Similar considerations apply to transport in other systems, such as carbon nanotube transistors and molecular wires in which the presence of a water layer affects the macroscopic characteristics of the device.<sup>25</sup> Correspondingly, the presence of a conductive water layer and associated alternative current paths will render transport measurements on CN-FET less reliable. In this case, mobile charge effects can be minimized using the variants of ac-EFM<sup>26</sup> or scanning impedance microscopy,<sup>27</sup> in which ac transport at relatively high frequencies (1–100 kHz) is measured. Because the oscillation period ( $\sim 10 \mu\text{s}$ –1 ms) is significantly smaller than the relaxation time of the mobile charges ( $\sim 1$ –1000 min), the charge-redistribution effects are minimized.

**Summary.** The grain boundary potential measured by SSPM is significantly smaller and opposite in sign to the grain boundary potential in the bulk. This behavior is shown to be due to screening at a surface–interface junction by mobile adsorbates. SPM-based dc and ac current measurements were shown to be relatively insensitive to the presence of the screening charge because of the large relaxation times of the latter. Similar behavior was observed for ferroelectric surfaces, on which the equilibrium surface potential, as observed by SSPM, has the sign of the screening charge rather than that of the polarization charge. These observations suggest that surface screening is a universal feature of oxide surfaces in air, and great care should be taken in the direct interpretation of the results of ambient electrostatic force-sensitive SPMs and SPM transport measurements.

**Acknowledgment.** D.A.B. acknowledges financial support from MRSEC grant NSF DMR00-79909 and DOE grant no. DEFG02-00ER45813-A001. Research was performed in part as a Eugene P. Wigner Fellow and staff member at the Oak Ridge National Laboratory, managed by UT-Battelle, LLC, for the U.S. Department of Energy under contract DE-AC05-00OR22725 (S.V.K.).

## References

- (1) Bridger, P. M.; Bandic, Z. Z.; Piquette, E. C.; McGill, T. C. *Appl. Phys. Lett.* **1999**, *74*, 3522.
- (2) Xu, Q.; Hsu, J. W. P. *J. Appl. Phys.* **1999**, *85*, 2465.
- (3) Chen, X. Q.; Yamada, H.; Horiuchi, T.; Matsushige, K.; Watanabe, S.; Kawai, M.; Weiss, P. S. *J. Vac. Sci. Technol., B* **1999**, *17*, 1930.
- (4) Tybell, T.; Ahn, C. H.; Triscone, J.-M. *Appl. Phys. Lett.* **1999**, *75*, 856.
- (5) Chavez-Pirson, A.; Vatel, O.; Tanimoto, M.; Ando, H.; Iwamura, H.; Kanbe, H. *Appl. Phys. Lett.* **1995**, *67*, 3069.
- (6) Meoded, T.; Shikler, R.; Fried, N.; Rosenwaks, Y. *Appl. Phys. Lett.* **1999**, *75*, 2435.
- (7) Kalinin, S. V.; Bonnell, D. A. *Z. Metallkd.* **1999**, *90*, 983.
- (8) Luo, E. Z.; Xie, Z.; Xu, J. B.; Wilson, I. H.; Zhao, L. H. *Phys. Rev. B* **2000**, *61*, 203.
- (9) Tanimoto, M.; Vatel, O. *J. Vac. Sci. Technol., B* **1996**, *14*, 1547.
- (10) *Scanning Probe Microscopy and Spectroscopy: Theory, Techniques and Applications*; Bonnell, D. A., Ed.; John Wiley: New York, 2000.
- (11) Dagata, J. A.; Schneir, J.; Harary, H. H.; Evans, C. J.; Postek, M. T.; Bennett, J. *Appl. Phys. Lett.* **1990**, *56*, 2001.
- (12) Garcia, R.; Calleja, M.; Perez-Murano, F. *Appl. Phys. Lett.* **1998**, *72*, 2295.
- (13) Domansky, K.; Leng, Y.; Williams, C. C.; Janata, J.; Petelenz, D. *Appl. Phys. Lett.* **1993**, *63*, 1513.
- (14) Sugimura, H.; Ishida, Y.; Hayashi, K.; Takai, O.; Nakagiri, N. *Appl. Phys. Lett.* **2002**, *80*, 1459.
- (15) Terris, B. D.; Stern, J. E.; Rugar, D.; Mamin, H. J. *Phys. Rev. Lett.* **1989**, *63*, 2669.
- (16) Cunningham, S.; Larkin, I. A.; Davies, J. H. *Appl. Phys. Lett.* **1998**, *73*, 123.

- (17) Buh, G. H.; Chung, H. J.; Kuk, Y. *Appl. Phys. Lett.* **2001**, *79*, 2010.
- (18) Nb-doped  $\Sigma 5$  SrTiO<sub>3</sub> bicrystals (1 at. %) were produced by diffusion bonding. A  $10 \times 10 \times 0.5$ -mm<sup>3</sup> crystal, which is dark blue because of donor doping, is sectioned such that the grain boundary is perpendicular to the (100) surface.
- (19) The AFM, EFM, and SSPM measurements were performed on a commercial instrument (Digital Instruments Dimension 3000 NS-IIIa) using a variety of probes. The lift height for the interleave scans was usually 100 nm. Measurements were performed using Au-coated cantilevers (spring constant  $k = 1-5$  N/m, NCSC 12 Cr-Au, Micromasch). The scan rate varied from 0.5 Hz for large scans ( $\sim 80$   $\mu$ m) to 1 Hz for smaller scans ( $\sim 10$   $\mu$ m). The driving voltage  $V_{ac}$  in the interleave scan was 5 V. The scan rate varied from 0.2 to 0.5 Hz. To reduce the effect of drift, the images were acquired with the grain boundary oriented along the slow scan axis. SSPM and EFM images were processed only by a background subtraction.
- (20) Kalinin, S. V.; Bonnell, D. A. *Phys. Rev. B* **2000**, *62*, 10419.
- (21) Kalinin, S. V.; Duscher, G.; Bonnell, D. A. To be submitted for publication.
- (22) Kalinin, S. V.; Bonnell, D. A. *Phys. Rev. B* **2001**, *63*, 125411.
- (23) Kalinin, S. V.; Johnson, C. Y.; Bonnell, D. A. *J. Appl. Phys.* **2002**, *91*, 3816.
- (24) Zeng, H. R.; Yin, Q. R.; Li, G. R.; Luo, H. S.; Xu, Z. K. *J. Cryst. Growth* **2003**, *254*, 432.
- (25) Kim, W.; Javey, A.; Vermesh, O.; Wang, Q.; Li, Y.; Dai, H. *Nano Lett.* **2003**, *3*, 193.
- (26) Bachtold, A.; Fuhrer, M. S.; Plyasunov, S.; Forero, M.; Anderson, E. H.; Zettl, A.; McEuen, P. L. *Phys. Rev. Lett.* **2000**, *84*, 6082.
- (27) Sergei Kalinin, V.; Dawn Bonnell, A. *Appl. Phys. Lett.* **2001**, *78*, 1306.

NL0350837